# Constant-Distance Mode Scanning Electrochemical Microscopy (SECM)—Part I: Adaptation of a Non-Optical Shear-Force-Based Positioning Mode for SECM Tips

**Bernardo Ballesteros Katemann, Albert Schulte, and Wolfgang Schuhmann*[a]**

**Abstract:** A non-optical shear-force-based detection scheme for accurately controlling the tip-to-sample distance in scanning electrochemical microscopy (SECM) is presented. With this approach, the detection of the shear force is accomplished by mechanically attaching a set of two piezoelectric plates to the scanning probe. One of the plates is used to excite the SECM tip causing it to resonate, and the other acts as a piezoelectric detector of the amplitude of the tip oscillation. Increasing shear forces in close proximity to the sample surface lead to a damping of the vibration amplitude and a phase shift, effects that are registered by connecting the detecting piezoelectric plate to a dual-phase analogue lock-in amplifier. The shear force and hence distance-dependent signal of the lock-in amplifier is used to establish an efficient, computer-controlled closed feedback loop enabling SECM imaging in a constant-distance mode of operation. The details of the SECM setup with an integrated piezoelectric shear-force distance control are described, and approach curves are shown. The performance of the constant-distance mode SECM with a non-optical detection of shear forces is illustrated by imaging simultaneously the topography and conductivity of an array of Pt-band microelectrodes.

**Keywords:** constant-distance mode · electrochemistry · microelectrodes · scanning electrochemical microscopy · scanning probe microscopy · shear forces

## Introduction

In scanning electrochemical microscopy (SECM), ultramicroelectrodes (UME) with micro- or even submicrometer-active tip diameters are employed as tiny electrochemical scanning probes (SECM tips). Images are acquired by laterally moving the SECM tip across the sample surface, usually at a constant height, and monitoring the amperometric or potentiometric tip response as a function of the tip position within the scanned area.[1] Since its inception about ten to fifteen years ago[2] a number of laboratories have made major contributions towards the development of the SECM.[3] SECM has matured into a valuable approach for probing and manipulating the solid/liquid interface.[1] Indeed, SECM has been successfully employed in a multitude of different applications such as mapping the local reactivity of (chemically modified) electrodes with high spatial resolution,[4] identifying and characterizing microscopic interfacial phenomena such as localized corrosion,[5] determining heterogeneous or homogeneous electron transfer kinetics,[6] imaging the activity of living biological cells,[7] and modifying and structuring surfaces on the micrometer scale.[8] For a comprehensive review of the basic principles of SECM and detailed information about the state-of-the-art SECM instrumentation and applications we refer to recently published monographs and review articles.[1, 9]

In general, SECM takes advantage of the strong dependence of the SECM tip response on the tip-to-sample distance ($d$) and the nature of the substrate with respect to its electrochemical activity/conductivity. For example, with a disk-shaped UME operated in the amperometric feedback mode, diffusion of electroactive species towards its sensing disk is hindered when it is in close proximity to an insulating target leading to a decrease in the tip current (negative feedback). Near to a conductor, electron transfer between the mediator and surface becomes possible allowing consumed redox species to be regenerated, subsequently increasing the tip current (positive feedback). The effects of negative and positive feedback can, in principle, be used to image the topography and local variations in the conductivity of sample surfaces. Imaging is usually performed by using so-called tip approach curves to position the SECM tip at a proper working distance at which the feedback effects occur, and then scanning the tip at a fixed height above the surface while simultaneously monitoring its current response as a function of $x$ and $y$ tip position.

[a] Prof. Dr. W. Schuhmann, Dr. B. Ballesteros Katemann, Dr. A. Schulte
Analytische Chemie—Elektroanalytik & Sensorik
Ruhr-Universität Bochum
Universitätsstrasse 150, 44780 Bochum (Germany)
Fax: (+49) 234-3214683
E-mail: Wolfgang.Schuhmann@ruhr-uni-bochum.de

 DOI: 10.1002/chem.200204267  

By applying constant-height mode SECM imaging to homogeneous surfaces (either fully conductive or insulating), their topography can be visualized because any change in the tip current then strongly relates to changes in *d*. In contrast, on flat samples with neighboring conductive and insulating regions, observed changes in the tip response reflect variations in conductivity. However, carrying out SECM in a constant-height mode has some major drawbacks. For instance, for samples that show local variations on both conductivity and topography, changes in the tip response arising from distance variations cannot, in general, be distinguished from those originating from alterations in conductivity, and additional information about the morphology of the specimen is required to allow a deconvolution of these two components. Additional problems arise due to the fact that the working distance suitable for successful imaging is strongly linked to the diameter of the active disk of the SECM tip. The working distance suitable for imaging has to be of the order of the diameter of the electrode used as the SECM tip. This is to ensure that either in the amperometric feedback mode the microelectrode tip is placed well within the regime of the negative and positive feedback effects or, in the generator/collector mode of operation, a good collection efficiency is guaranteed.[10] There is a risk of tip crash when the tip is scanned at constant height across a tilted surface (Figure 1 A) or when the height of three-dimensional structures on the sample surface significantly exceeds the diameter of the SECM tip itself (Figure 1 C). On the other hand, the feedback or collection efficiency is lost if the tip is scanned away from a tilted surface (Figure 1 B) or during scanning across grooves or holes (Figure 1 D). As a matter of fact, scanning at constant height becomes more difficult and the probability of a tip crash increases if the size of the SECM tip is reduced in the hope of attaining higher resolution imaging.

**Abstract in German:** *Scherkraftwechselwirkungen, die bei sehr geringen Abständen zwischen in Resonanz schwingenden, nadelförmigen Mikroelektroden und der Probenoberfläche auftreten, wurden für die Entwicklung eines nicht-optischen Verfahren zur präzisen Abstandskontrolle von Messsonden für die elektrochemische Rastermikroskopie (SECM) verwendet. Eine hochempfindliche Detektion der Scherkräfte gelang dabei durch zwei in geeigneter Weise an den Sonden befestigte piezoelektrische Plättchen, von denen eines zur Anregung der Schwingung und das zweite zur Detektion der Schwingungsamplitude und -phase mittels eines Lock-In Verstärkers verwendet wird. Auf Basis des scherkraft- und damit auch abstandsabhängigen Signals des Lock-In Verstärkers konnte eine leistungsfähige rückgekoppelte Regelung etabliert werden, die eine kontinuierliche Repositionierung der SECM-Sonden während des Rasterns über der Probenoberfläche gewährleistet und dadurch einen Betrieb des SECM im "constant-distance" Modus möglich macht. Alle wichtigen technischen Details des SECM mit integrierter piezoelektrischer Höhenkontrolle werden ausführlich beschrieben. Außerdem werden Scherkraftabhängige und elektrochemische Annäherungskurven gezeigt und die Vorteile eines Betriebes im "constant-distance" Modus durch eine simultane Abbildung sowohl der Topographie als auch der Leitfähigkeit eines bandförmigen Mikroelektrodenarrays veranschaulicht.*

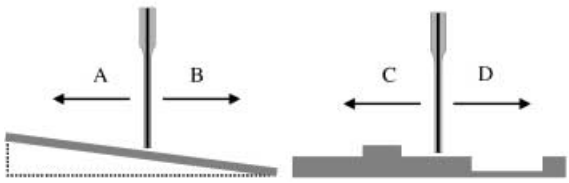


Figure 1. Principle limitation of SECM measurements using a SECM tip scanned at constant height on a tilted surface (A,B) and on surfaces with three-dimensional features (C) or grooves and holes (D). Tip crash will occur in A and C, while a loss of the near-field distance will take place in B and D.

Because of the principal limitations of the constant-height mode of operation, constant-distance mode SECM was considered important as it guarantees knowledge and control of the tip-to-sample distance, both fundamental prerequisites for an unambiguous interpretation of SECM data and for avoiding tip crash. As scanning at a constant distance forces the SECM tip to follow the contours of the surface, it not only allows simultaneous acquisition of the electrochemical tip response and the sample topography but also prevents tip crash even with very small SECM tips. For the reasons mentioned above, the amperometric SECM tip current is not suitable for providing input for a closed-loop feedback control that could be used to maintain a constant distance of the tip to the specimen during electrochemical imaging. After attempts to control the tip-to-sample distance using tip modulation[11] or picking modes,[12] it became obvious that the convolution between distance and electrochemical activity can only be resolved by using non-electrochemical strategies for SECM imaging in a constant-distance mode. In 1995, we showed for the first time that a shear-force-based feedback mechanism with an optical detection system, as originally developed by others for the positioning of ultrasmall optical fiber tips in scanning near-field optical microscopy (SNOM),[13] can also successfully be adapted to control and regulate the tip-to-sample distance in SECM.[14] With this technique, a flexible SECM tip is vibrated laterally at its resonant frequency using a piezoelectric buzzer for agitation. By focusing a laser beam on the vibrating probe tip and projecting the resulting Fresnel diffraction pattern onto a split photodiode, the amplitude of the tip oscillation could be monitored optically by a phase-sensitive amplification of the difference signal of the photodiode with respect to the agitation signal using a lock-in amplifier. As the oscillating SECM tip approaches the sample surface, the amplitude of vibration is observed to decrease at very close distances due to increasing shear forces occurring in the near-field regime of the sample ($\ll 1$ μm). To accomplish constant-distance mode SECM, the tip is positioned at a distance at which a predefined value of damping is reached (set point). A computer-controlled closed-loop feedback during scanning continuously compares the actual value of the vibration amplitude with the set point value, and it responds rapidly to any resulting differences (reflecting distance variations) by readjusting the tip-to-sample distance using the z-positioning elements of the SECM setup. This guarantees the maintenance of a constant level of damping and noncontact scanning at a constant distance of much less

than one micrometer. An alternative way to achieve shear-force-based constant-distance mode SECM has been described by Smyrl et al.[15] They attached the SECM tip to the tuning fork resonance detection system of a commercially available SNOM and used the response of the tuning fork/SECM tip-assembly as a measure of shear-force-induced damping of the tip vibration and as an input for a feedback control. However, due to the fact that the SECM tip is not vibrating at its resonant frequency, the shear-force interaction occurs only at shorter distances between the UME and the sample surface. In addition, the higher stiffness of the tips used does not allow the visualization of soft sample surfaces. More recently, an electrochemical impedance method for controlling the tip-to-sample separation in SECM was proposed.[16] With this method, a small sinusoidal voltage is applied to the SECM tip causing an alternating current (AC) to flow between the tip and a counter electrode. This current is affected by the tip-to-sample distance and was used to establish a feedback loop allowing the SECM tip to scan at constant distance. Furthermore, the functionality of a SECM was integrated into a commercially available atomic force microscope (AFM) by using specially designed AFM cantilevers. These acted as both a force sensor for topographical imaging and a UME for electrochemical measurements.[17] However, it has to be pointed out that the components needed to operate a shear-force-based constant-distance SECM can be integrated easily into conventional SECM setups, thus avoiding the need to invest in AFM equipment. In addition, the $z$ range and the $x$,$y$ scanning area of commercial AFM systems is often limited and the integration of fully functioning electrochemical cells suitable for non-flat samples is often difficult.

Shear-force-based constant-distance SECM with an optical detection scheme for the shear forces has already been successfully used for surface modification,[14b] the positioning of non-amperometric SECM tips,[14c] and measurements on soft biologial samples, that is, for imaging the topography and activity of single secretory cells.[7g] However, the optical shear-force detection system requires a number of presuppositions for the design of the setup. The SECM tip has to be kept in a fixed position to ensure a permanent and perfect alignment with the laser beam and the photodiode. Consequently, the assembly for holding the tip with the agitation piezo, the laser, and the photodiode have to be arranged on a rigid metal plate and the sample has to be moved in the $x$,$y$,$z$ direction with a fixed-tip configuration. A specially designed chamber with two parallel glass windows of high quality and clear, transparent electrolytes are needed to allow the laser beam to pass through the electrochemical cell unaffected. Furthermore, the laser beam should be positioned as close as possible to the very end of the SECM tip to be most sensitive to shear forces but not too close to avoid disturbances of the optical signal due to reflection of light from the sample surface.

Although it works very well, at least for conventional SECM tips with typical diameters of 5–25 μm, the setup with an optical detection of shear forces and its operation is rather complicated and needs a lot of hands-on experience. To simplify shear-force-controlled constant-distance SECM, we have developed a highly sensitive, non-optical shear-force distance control for SECM tips as an easier-to-use alternative to the optical method. The method is adapted to the specific needs of SECM from an earlier work by Brunner and Marti in which a piezoelectric shear-force distance control for SNOM was described.[18] They sandwiched the holder for a tapered optical fiber between two piezoelectric plates; one of these was used to excite the fiber tip to oscillate at resonant frequency, the other detected the amplitude of tip vibration. However, due to the characteristics of the SNOM tips used, the proposed system was optimized for operation in air or in liquid films of small height.

Herein, we report on the integration of a variant of this method into a specifically designed SECM setup. To make the piezoelectric system function, we had to adapt it to the special requirements arising from the fact that disk-shaped voltammetric ultramicroelectrodes of different design are used. These are quite different from the tapered optical fibers used for SNOM, mainly in terms of their stiffness, the length of the pulled capillary, and, most importantly, the insertion depth into the electrolyte solution. All important technical aspects of the SECM setup with the piezoelectric shear-force distance control are given below, including a detailed description of how to operate the non-optical constant-distance mode SECM. The performance of the method is finally illustrated by imaging simultaneously the topography and conductivity of an array of Pt-band microelectrodes.

## Results and Discussion

**Technical concept of a SECM with an integrated, non-optical shear-force-based distance control**: Figure 2 shows a sche-

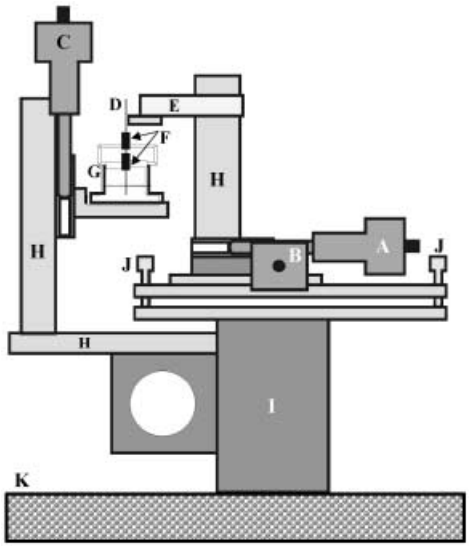


Figure 2. Schematic representation of the basic design of the SECM instrument as used with a non-optical, piezoelectric shear-force distance control. A,B) Stepper motors and piezoelectric stacks for $x$ and $y$ tip displacements; C) stepper motor and a piezoelectric stack for $z$ positioning of the electrochemical chamber; D) SECM tip/microelectrode; E) tip holder; F) agitation and detection piezoelectric plate; G) electrochemical chamber; H) rigid metal holders; I) base plate; J) set of three screws for the compensation of a tilt possibly be present between the plane of the microdisk of the SECM tip and the plane of scanning; K) vibration damping table.

  

matic representation of the compact design of our specifically designed SECM setup with an integrated, non-optical shear-force distance control. Because a piezoelectric and not an optical read-out of shear forces is used to operate the shear-force-based distance control, no laser has to be focused on the very end of the SECM tip or aligned with a photodiode. Thus, no special electrochemical chamber equipped with glass windows is necessary, and a fixed-tip configuration is not required either. This allowed us to establish a micropositioning system with which the SECM tip is moved in the $x$ and $y$ directions for scanning the surface of the sample, whereas the electrochemical cell with the sample fixed to its bottom is moved in the vertical ($z$) direction for tip approach and control of the tip-to-sample distance.

The electrochemical cell including the sample, reference, and counter electrode is mounted on a one-axis translation stage ($z$) driven by a robust, computer-controlled stepper motor. This allows translation of the sample towards or away from the SECM tip. To allow the detection of shear forces between a vibrating SECM tip and the sample surface, highly flexible disk-shaped Pt microelectrodes are needed which were fabricated from Pt wires of 10 μm diameter sealed into the tapered end of pulled glass capillaries.[14] Varying the length of the tapered region and the diameter of the insulating sheath allowed adjustment of the stiffness of the glass-insulated Pt microelectrodes in such a way that SECM tips with characteristic resonant frequencies from only several hundred Hz up to about 150 kHz became available. These SECM tips were mounted by using a rigid tip holder to two additional translation stages ($x$,$y$), again both driven by a set of computer-controlled stepper motors and used for scanning in the $x$,$y$ direction. The stepper motors provided an approximate $x$, $y$, and $z$ positioning with a spatial resolution of 0.6 μm per half step and the advantages of a long travel path (2.5 cm). However, for an accurate and fast control of the tip-to-sample distance (fine positioning of the $z$ height) in a closed-loop feedback control, and for rapid and precise movements of the sample in the $x$,$y$ direction, three piezoelectric stacks were included additionally into all three translation stages. These allowed displacements with a nominal resolution of 3–5 nm in each direction.

The key component of the SECM setup with a non-optical, shear-force based constant-distance control is the integrated, piezoelectric shear-force detection system, which consists essentially of two thin piezoelectric plates and one or two tiny blocks of brass. The brass blocks have a cylindrical hole drilled through their center from the top, just large enough in diameter to allow a Pt microelectrode (SECM tip) to be inserted and kept in place at various positions along the electrode body using a pair of small set screws. In our first attempts to construct the shear-force detection system we precisely followed the geometry of the arrangement as described earlier by Brunner and Marti for optical fiber tips in SNOM[18] (see Figure 3A). Two piezoelectric plates were attached sandwichlike to the opposite faces of one of the specially designed brass holders and the holder was then fixed to a metal tube at the taper of the Pt microelectrode. The metal tube was glued to the narrowing part of a glass-insulated Pt microelectrode in such a way that about 2 mm of the glass

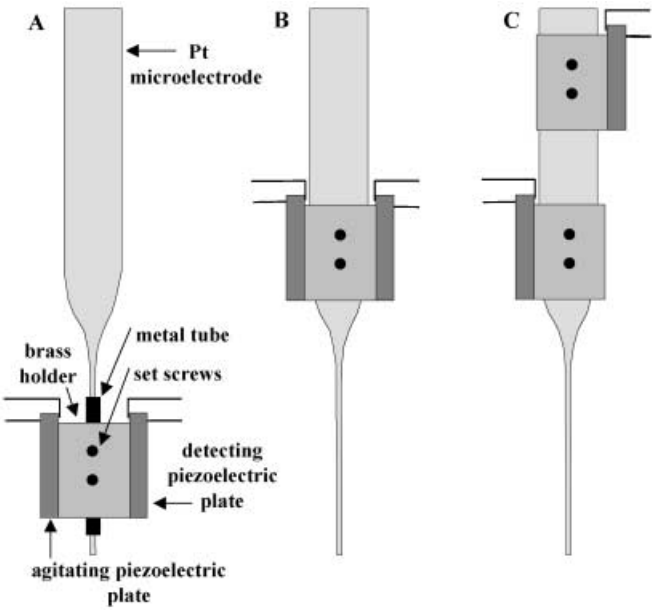


Figure 3. Schematic representation of the different assemblies of an SECM tip, one or two brass holders, and two piezoelectric plates as used for the implementation of a non-optical shear-force-based distance control into an SECM. A) The design as proposed by Marti and Brunner[18] for the positioning of optical fiber tips in SNOM; B,C) Two modifications of the design as shown in A) with the brass holder simply fixed at a different position of the microelectrode body (B) or with a separation of the piezoelectric plates used for agitation of tip vibration and detection of the amplitude of tip vibration (C).

tip was protruding out of it and protected the fine glass structure from breaking when using the set screws of the brass holder for fixation. To complete the system, one of the piezoelectric plates was connected to a function generator allowing the application of small sinusoidal voltages to excite the SECM tip/brass holder assembly to vibration at resonant frequency. The second piezoelectric plate was connected to a lock-in amplifier and a phase-sensitive amplification of its alternating voltage was used to monitor the amplitude of the SECM tip oscillation. (The amplitude of the AC voltage of the detecting piezoelectric plate as measured with the lock-in amplifier is abbreviated as $V_{piezo}$ in the following description.)

To test the performance of this arrangement, frequency spectra were recorded and used to determine a suitable resonant frequency for glass-insulated Pt microelectrodes before finally approach curves (plots of $V_{piezo}$ versus $d$) were acquired with the tip vibrating at resonance to check the ability of the system to detect shear forces. However, the arrangement successfully used for optical fiber tips turned out to be unsuitable for SECM tips for the following reasons. First, it was rather difficult to find appropriate resonant frequencies for the brass holder/SECM tip assembly, and if found, the system was rather insensitive to the shear forces occurring between the microelectrode tip and the sample. This might be explained by the different geometry of tapered optical fibers and Pt microelectrodes and the fact that a Pt wire is sealed into the glass tips, both of which possibly lead to significant differences in their mechanical stiffness and vibration characteristics as compared to conventional opti-

cal-fiber tips. Moreover, with the piece of brass fixed to the thin glass tips, the assembly was very fragile and for that reason difficult to handle. Even when special care was taken, the fine glass tips often were liable to break during fixation of the brass holder or when the assembly was inserted into the SECM.

To develop a system that showed both improved sensitivity to shear forces and decreased fragility, several other designs for assembling the brass holder and the piezoelectric plates for agitation and detection were investigated. For example, a brass holder with the two piezoelectric plates opposing each other was fixed to the upper part of the microelectrode body just above the region where the pulled capillary starts to get thinner (see Figure 3B). This lowered the risk of breaking the glass tips of the microelectrodes, however, it did not allow detection of shear forces with the tip in the near-field regime of the sample. In our final attempt, the detection and agitation piezoelectric plates were glued separately to two brass holders which were then fixed to the microelectrode body in such a manner that the piezoelectric plates were located oppositely at either side of the glass capillary (see Figure 3C). In fact, with such a design it became possible to excite the microelectrode tip adequately to vibrate at resonance, and, even more importantly, the amplitude of the tip vibration became very sensitive to the appearance of shear forces. Figure 3 shows a schematic diagram of the non-optical shear-force-based distance control as finally successfully employed for the accurate positioning of SECM tips and for SECM imaging in a constant-distance mode of operation.

**Frequency spectra and approach curve measurements**: Frequency spectra were recorded with the system as shown in Figure 4 and used to determine suitable resonant frequencies for the disk-shaped Pt microelectrodes. Usually, two spectra were measured, one with the entire assembly kept in air and another one, using the SECM device for tip positioning, after immersing just the very end of the microelectrode tip into water. As can be seen from Figure 5, the two spectra are rather complex and indistinguishable for most of the frequencies. However, at certain frequencies (indicated with arrows in Figure 5) significant differences in $V_{piezo}$ occurred. The amplifier's output at these characteristic frequencies was usually reduced upon immersion, an effect that can be attributed to a damping of the tip vibration. Since the output of the lock-in amplifier at these frequencies depended strongly on interactions of the tip with the liquid environment, no others were considered important to establish a shear-force-based feedback. With the tip just a few tenths of a micrometer above the surface of the sample but surely out of the regime of shear forces, a fine tuning of the frequencies of choice was used to further optimize the response of the detecting piezoelectric plate and the lock-in amplifier signal. This ensured that during an approach the degree of damping by changing the immersion depth of the tip was negligible as compared with the degree of damping that occurred upon final surface approach. With these settings, a series of approach curves was performed, all under exactly the same experimental conditions but with the difference that the tip was brought to vibration in each case with one of the shear force-sensitive frequencies as determined from the frequency spectra. From the appearance of these approach curves, the

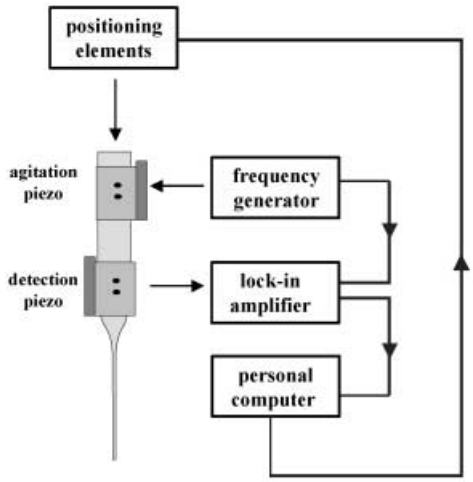


Figure 4. Illustration of the piezoelectric shear-force detection system as used successfully in this study to establish constant-distance mode SECM.

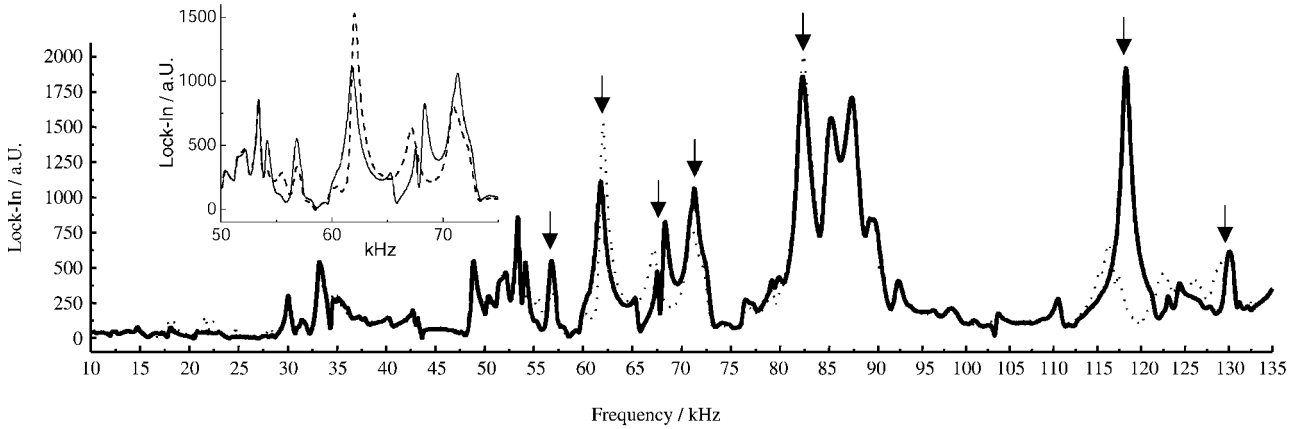


Figure 5. Frequency spectra (10–135 kHz) of a glass-insulated 10 μm diameter Pt-disk microelectrode integrated into the piezoelectric shear-force detection system as shown in Figure 3C and measured with the microelectrode kept above a solution in air (solid line) and with just the very end of the tip of the microelectrode immersed into the electrolyte (dashed line). The arrows indicate frequencies at which the two superimposed spectra differ significantly from each other.

  

frequency offering the best sensitivity for a detection of shear forces was selected and used for establishing the shear-force-dependent feedback loop for constant-distance SECM.

Figure 6 shows the overlay of a typical electrochemical and a shear-force-based approach curve, simultaneously recorded with a disk-shaped Pt microelectrode (10 μm in diameter, part

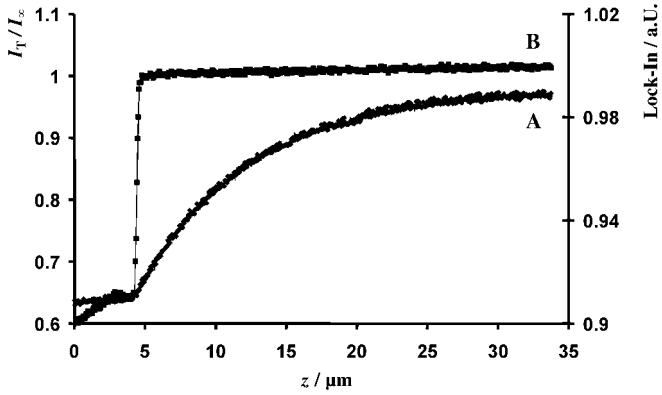


Figure 6. Approach curves of a glass-insulated 10 μm diameter Pt-disk microelectrode obtained at an insulating surface (epoxy) in a solution of 5 mM $[Ru(NH_3)_6]Cl_3$ and 0.5 mM KCl. A) Diffusion-controlled steady-state tip current with the microelectrode held at −300 mV versus Ag/AgCl reference as a function of tip-to-sample distance; B) simultaneously recorded amplitude of the tip vibration (measured with the piezoelectric shear-force detection system as shown in Figure 3) versus tip-to sample distance.

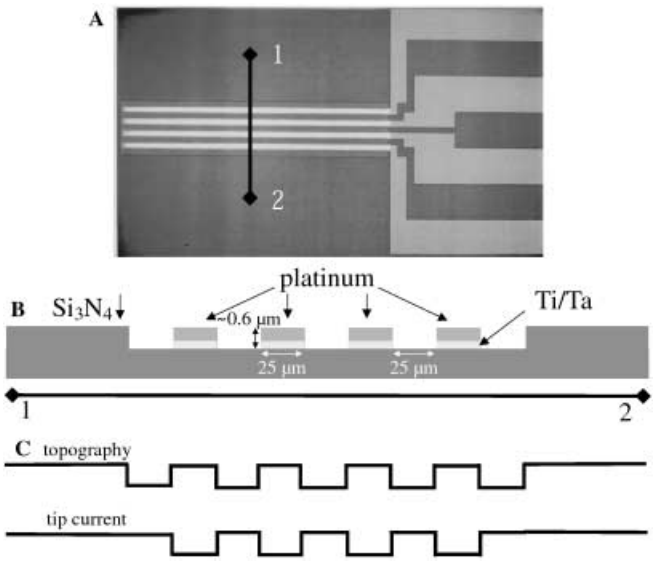


Figure 7. A) Light microscopy picture of the Pt microband array used as model sample; B) schematic representation of the topography and conductivity properties of a cross section of the sample along the line from point 1 to point 2; C) schematic depiction of the expected topography and current response during a SECM line scan in constant-distance mode along the line from point 1 to point 2. The increase in the cathodic current due to positive feedback above the platinum is seen as a downward deflection in the current trace.

of a piezoelectric shear-force detection system as shown in 3 C and vibrated laterally to resonance at 80 kHz) throughout the approach to an insulating surface. As expected, the amperometric current response of the microelectrode starts to decrease at distances below about 30 μm on account of the effect of negative feedback (modulation of the hemispherical diffusion profile in front of the microelectrode). In contrast, the shear-force-induced damping of the tip vibration takes place at much shorter distance, typically at distances of less than 500 nm.

**SECM imaging in the shear-force-based constant-distance mode**: The feasibility of the developed shear-force-based constant-distance mode with a non-optical detection of the shear force was evaluated by imaging simultaneously the topography and conductivity of a model sample consisting of an array of Pt-band microelectrodes with four parallel bands, each of them 1 mm in length, 25 μm in width, and with a 25 μm insulating space in between them. The height of the Pt microstructures was determined by means of AFM line scan measurements (not shown) and was found to be about 0.6 μm. A light microscope picture and a schematic representation of the model sample together with the expected topographic and tip current response for SECM imaging in the constant-distance mode are shown in Figure 7.

Prior to imaging in the constant-distance mode of operation, the computer-controlled feedback loop constantly regulating the tip-to-sample separation during scanning had to be established. Following the procedure as described above, the SECM tip, a 10 μm Pt-disk microelectrode, was made to vibrate at a suitable, shear-force sensitive frequency. Then, the electrochemical cell with the sample was moved towards the vibrating probe tip at an intermediate speed of about 1–5 μm $s^{-1}$, while continuously monitoring the amperometric tip current and the amplitude of tip vibration, $V_{piezo}$, over time.

As a matter of fact, the reduction in the tip current due to negative feedback appeared notably earlier than the decrease of the vibration amplitude due to shear forces. Accordingly, the tip current could be taken as a first indication that the probe became close to the surface and at the time when the tip current was starting to decrease, the speed of approach was reduced to much slower values of only about 100–200 nm $s^{-1}$ to assure a very gentle positioning of the scanning probe into the regime of shear forces. The attentive $z$ approach was automatically stopped at a user-defined degree of damping of the vibration amplitude (at the "set point"), usually at 70–80 % of the unaffected value with the tip far above the surface. The developed SECM software allowed determination of the slope ($\Delta V_{piezo}/\Delta z$) at the end of the approach curve, which in principle defines a linear function between the damping of the vibration amplitude and the displacements in the $z$ direction. The derivative $\Delta V_{piezo}/\Delta z$ allowed the sensitivity of the closed-loop feedback control to be set. This permitted it to respond instantly to changes in the amplitude of tip oscillation ($\Delta V_{piezo}$, indicating increasing or decreasing shear forces due to variations in $d$) with readjustment of the tip-to-sample distance by driving the $z$-positioning element of the system exactly the corresponding $\Delta z$. A so-called damping factor was integrated into the module of the SECM software running the feedback loop and ensured that it was not overacting in terms of over-swinging around the set point, as often happens for

such feedback control schemes. Clearly, the damping factor slows down the response of the established feedback loop to changes occurring in the sample's morphology. By means of a proper setting of the damping factor it was ensured that the damping of the feedback loop did not lead to a poor and slow response to changes in the topography of the sample, and over-swinging did not hinder successful imaging. Once the feedback loop was optimized, SECM imaging in the constant-distance mode of operation could be started. Usually, imaging in constant-distance mode was performed at a speed of 0.1–10 μm $s^{-1}$ for $x$ and $y$ displacements (depending on the desired resolution). In the background, the stable feedback loop continuously guaranteed the maintenance of a constant tip-to-sample distance within the regime of shear forces, namely of about 100–200 nm.

Figure 8 illustrates the current (A) and the topographical (B) images of the array of Pt-band microelectrodes, acquired simultaneously by using the SECM in the constant-distance mode as described above. The topographic and current values of the forward and backward scans were recorded (backward image not shown). The images did not differ from each other and gave identical height and current profiles of the test structure. The current image corresponds well with the topographical image (compare also the schematic representation of the structure in Figure 7) and the electrochemical and morphological properties of the four Pt-band microelectrodes were visualized in a very sensitive way with high contrast. Evidently, as the overall diameter of the tip electrode (about 100 μm) is much larger than the clearly resolved microstructure, the shear-force interaction occurs between a protruding edge of the microtip and the sample surface.

The obtained results clearly demonstrate the ability of the shear-force-dependent feedback loop with a piezoelectric detection of the shear forces to resolve the topographical fine structure of the model substrate and underline the performance of the non-optical approach for the detection of shear forces. Notably, the topography image displayed a relative upward movement of the scanning probe in the $x$ and $y$ directions with a difference in the height of more than a few μm within the scanned range. This displacement is the result of a surface tilt of the sample relative to the plane of $x$,$y$ scanning and its visualization should be seen as further proof that the shear-force-dependent feedback loop certainly was forcing the SECM tip to follow the contours of the tilted surface. Since the SECM tip was scanned at a constant distance, the tilt of the sample surface did not influence the electrochemical response (corresponding to the level of negative/positive feedback) throughout scanning. For instance, the values of the current with the tip above the insulating parts at the beginning and the end of the scans were almost identical to each other (see Figure 8A and 9A). As

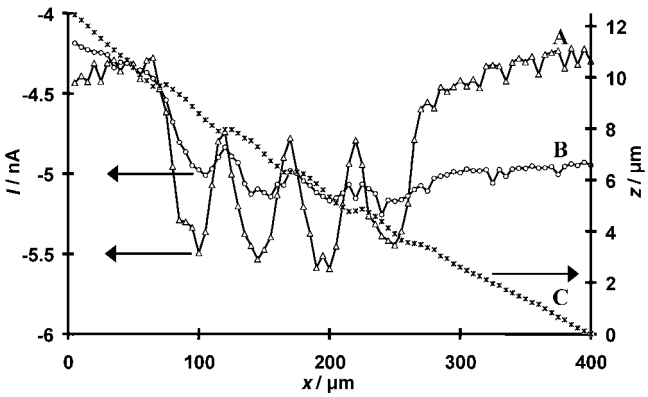


Figure 9. Single current line scans obtained during scanning of a 10 μm diameter Pt-microelectrode across an array of Pt-band microelectrodes by using SECM either in A) a constant-distance or B) a constant-height mode and displaying the amperometric tip response (left axes) versus $x$ position. The parameters for SECM imaging were the same as in Figure 6. C) Topographical line scan (displacement of the $z$-positioning element (right axes) versus $x$ position) acquired together with the current scan as shown in A).

one can see from Figure 9B, this is not observed when the imaging procedure was performing by using the SECM in the conventional constant-height mode of operation with which the SECM tip is first positioned at a proper working distance and then scanned at a fixed setting of the $z$-positioning

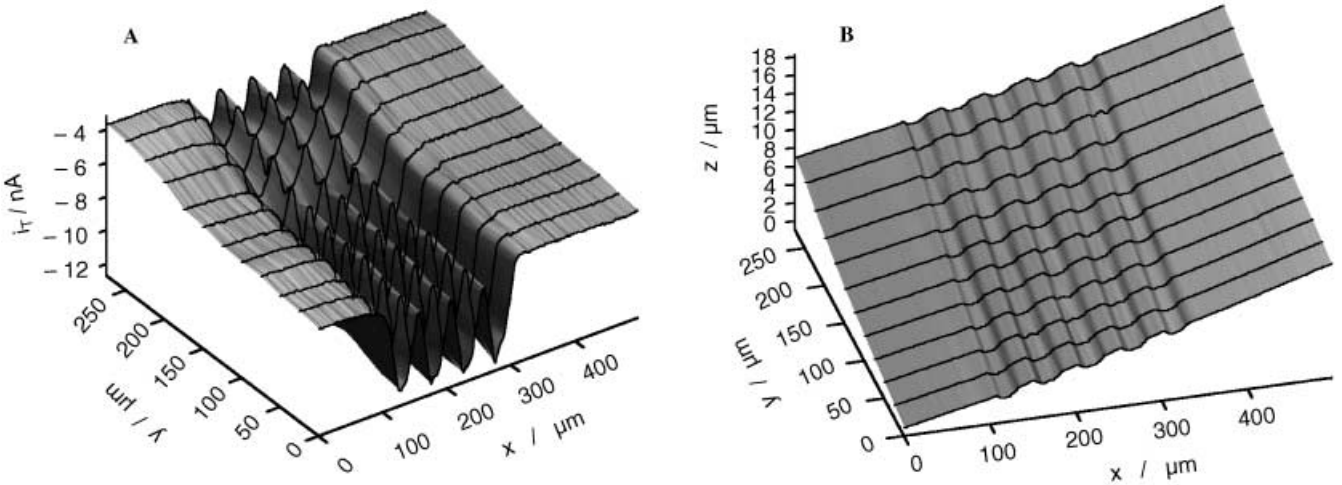


Figure 8. A) Amperometric feedback and B) topographic images of a 500 × 250 μm portion of an array of Pt-band microelectrodes. Both images were acquired simultaneously in a solution of 5 mM $[Ru(NH_3)_6]Cl_3$ and 0.5 mM KCl with a 10 μm diameter Pt-disk microelectrode vibrating at resonance and kept at −300 mV versus Ag/AgCl serving as the scanning probe for imaging with constant-distance mode SECM.

  

element of the device. Scanning the tilted surface of the Pt-band electrodes at constant height continuously led to changes in the tip-to-sample distance. In turn, this varied the degree of electrochemical feedback and hence the amperometric tip current. Consequently, employing the constant-distance mode of SECM offered the major advantage that an improved electrochemical image of the Pt band microelectrodes with a much better contrast between the insulating and conducting regions was obtained simultaneously with an image of the morphology of the sample surface.

## Conclusion

A non-optical shear-force-based detection scheme for maintaining a constant tip-to-sample distance in SECM has been presented. The appearance of shear forces between the SECM tip and the sample surface has been measured with a high sensitivity by using two piezoelectric plates one of which was used to stimulate the tip to vibration at resonance, while the other was connected to a lock-in amplifier and a phase-sensitive amplification of its alternating voltage was used to monitor the amplitude of the tip oscillation. As the vibrating SECM tip got into very close proximity of the sample surface, increasing shear forces led to a damping of the vibration amplitude that was clearly observed as a decrease of the output of the lock-in amplifier. The distance dependence of the amplitude of tip oscillation allowed a computer-controlled closed-loop feedback to be established, which constantly regulated the tip-to-sample spacing throughout scanning to only a fraction of a micrometer. Thus, SECM in a constant-distance mode of operation became possible, providing independent information about the sample topography and its electrochemical activity/conductivity. The viability of the method has been unequivocally proven by imaging, at the same time, both the topography and conductivity of an array of Pt-band microelectrodes and by comparing the current images with ones acquired using SECM in a constant-height mode. The measurements in the constant-distance mode produced better-quality current images of the Pt band microelectrodes with an enhanced contrast between the insulating and conducting regions. The non-optical detection of shear forces offers the advantage over our recently published optical approach in that it is easier to use and the operator is not limited to special electrochemical chambers and transparent solutions. Furthermore, a piezoelectric detection of shear forces should be suitable for the positioning of ultrasmall SECM tips[19] with significantly reduced total tip diameters compared to those needed for high-resolution topographical imaging. The high-resolution imaging with glass-insulated Pt nanoelectrodes as the scanning probes operated by employing constant-distance mode SECM with a non-optical detection of shear forces is currently under investigation.

## Experimental Section

**Chemicals, samples, and microelectrode preparation**: All SECM experiments were performed in aqueous solutions containing 5 mM $[Ru(NH_3)_6]Cl_3$ (Strem Chemicals, Newburyport, MA, USA) in 0.1 M KCl (Riedel de Haen, Seelze, Germany). The samples studied were arrays of Pt microband electrodes prepared by using standard lithographic procedures with four parallel bands, each of them about 1 μm in height, 1 mm in length, 25 μm in width, and with a 25 μm insulating space in between them. Glass-insulated, disk-shaped Pt microelectrodes 10 μm in diameter with a ratio between the diameter of the active surface to the insulating glass sheath of about 10 (not exactly determined) have been used as SECM tips and were fabricated from platinum wires 10 μm in diameter (Goodfellow, Bad Nauheim, Germany) sealed into the tapered tips of pulled borosilicate capillaries (Hilgenberg, Art. No. 1400372, Hilgenberg, Germany; O.D.: 1.5 mm, I.D.: 0.75 mm) following a procedure described previously.[14]

**Instrumentation, SECM components**: SECM imaging was carried out in a one-compartment electrochemical cell and in three-electrode configuration, with the SECM tip acting as working (WE), a Pt-wire as counter electrode (CE) and a chlorinated silver wire as a Ag/AgCl pseudo-reference electrode (RE).

A PC in combination with Windows software programmed in Microsoft Visual Basic 3.0 (Microsoft, Unterschleißheim, Germany) was used for the control of all system parameters and for data acquisition. Accurate control of the potential of the SECM tip was provided by a bipotentiostat/galvanostat (PG 100, Jaissle Elektronik GmbH, Waiblingen, Germany) capable of measuring currents in the sub-nA range at low-noise. The main components of the micropositioning device of the SECM were three translation stages (Owis, Staufen i. Br., Germany) and three computer-controllable stepper motors with a nominal resolution of 0.6 μm per half step and a maximal travel path of about 2.5 cm (Owis, Staufen i. Br., Germany), together with three piezoelectric stacks from Piezomechanik Pickelmann GmbH, München, Germany. The piezoelectric devices offered maximal displacements of either 80 μm (the ones used for scanning in the *x*,*y* direction) or 40 μm (the one used for tip movements in the *z* direction/tip approach) at 150 V and were driven by a computer-controlled high-voltage power supply (PS500/5; Owis, Staufen i. Br., Germany). The tip-holding assembly including the piezoelectric shear-force detection system was built from a home-made brass holder ($4 \times 2 \times 3.5$ mm) and two piezoelectric plates of 0.5 mm thickness (Piezomechanik Pickelmann GmbH, München, Germany). A function generator (HP 33120A, Hewlett-Packard, USA) was connected to one of the piezo plates and used to stimulate the SECM tip oscillation. The second piezo plate was used to detect the amplitude of the vibration of the SECM tip, and therefore connected to a dual-phase analogue lock-in amplifier (PAR5210, Perkin Elmer, Bad Wildbad, Germany).

## Acknowledgement

This work was in part financially supported by the Deutsche Forschungsgemeinschaft (DFG) (Schu 929/5 – 1; SFB 459, A5), the Volkwagenstiftung (I/72612). The authors are grateful to Prof. Milena Koudelka-Hep, IMT, University of Neuchâtel for supplying the microband arrays. Furthermore, we thank the workshop staff at the Faculty of Chemistry at the Ruhr-Universität Bochum, especially Armin Lindner, for their helpful input in building up the described SECM instrument.

[1] *Scanning Electrochemical Microscopy*, (Eds.: A. J. Bard, M. V. Mirkin), Marcel Dekker, Inc. New York, **2001**

[2] a) R. C. Engstrom, C. M. Pharr, *Anal. Chem.* **1989**, *61*, A 1099 – A 1104; b) A. J. Bard, F. R. F. Fan, J. Kwak, O. Lev, *Anal. Chem.* **1989**, *61*, 132 – 138; c) A. J. Bard, F. R. F. Fan, D. T. Pierce, P. R. Unwin, D. O. Wipf, F. Zhou, *Science* **1991**, *253*, 68 – 74.

[3] a) A. J. Bard, G. Denuault, R. A. Friesner, B. C. Dornblaser, L. S. Tuckerman, *Anal. Chem.* **1991**, *63*, 1282 – 1288; b) K. Borgwarth, C. Ricken, D. G. Ebling, J. Heinze, *Ber. Bunsenges. Phys. Chem.* **1995**, *99*, 1421 – 1426; c) D. Mandler, S. Meltzer, I. Shohat, *Isr. J. Chem.* **1996**, *36*, 73 – 80; d) B. R. Horrocks, M. V. Mirkin, D. T. Pierce, A. J. Bard, G. Nagy, K. Toth, *Anal. Chem.* **1993**, *65*, 1213 – 1224; e) G. Wittstock, H. Emons, T. H. Ridgway, E. A. Blubaugh, W. R. Heineman, *Anal. Chim. Acta* **1994**, *298*, 285 – 302; g) S. Meltzer, D. Mandler, *J. Electrochem. Soc.* **1995**, *142*, L 82 – L 84; f) S. Nugues, G. Denuault, *J. Electroanal.*

  

*Chem.* **1996**, *408*, 125–140; g) O. D. Uitto, H. S. White, *Anal. Chem.* **2001**, *73*, 533–539.

[4] a) M. Arca, M. V. Mirkin, A. J. Bard, *J. Phys. Chem.* **1995**, *99*, 5040–5050; b) B. Gründig, G. Wittstock, U. Rudel, B. Strehlitz, *J. Electroanal. Chem.* **1995**, *395*, 143–157; c) G. Wittstock, W. Schuhmann, *Anal. Chem.* **1997**, *69*, 5059–5066; d) C. Kranz, T. Lötzbeyer, H.-L. Schmidt, W. Schuhmann, *Biosens. Bioelectron.* **1997**, *12*, 257–266; e) C. Kranz, G. Wittstock, H. Wohlschläger, W. Schuhmann, *Electrochim. Acta* **1997**, *42*, 3105–3111; f) D. J. Strike, A. Hengstenberg, M. Quinto, C. Kurzawa, M. Koudelka-Hep, W. Schuhmann, *Mikrochim. Acta* **1999**, *131*, 47–55; g) M. Tsionsky, J. F. Zhou, S. Amemiya, F. R. F. Fan, A. J. Bard, R. A. W. Dryfe, *Anal. Chem.* **1999**, *71*, 4300–4305; h) A. R. Kucernak, P. B. Chowdhury, C. P. Wilde, G. H. Kelsall, Y. Y. Zhu, D. E. Williams, *Electrochim. Acta* **2000**, *45*, 4483–4491; i) F. Y. Ge, R. C. Tenent, D. O. Wipf, *Anal. Sci.* **2001**, *17*, 27–35; k) T. Wilhelm, G. Wittstock, *Electrochim. Acta* **2001**, *47*, 275–281.

[5] a) D. O. Wipf, *Colloid Surf. A-Physicochem. Eng. Asp.* **1994**, *93*, 251–261; b) N. Casillas, S. Charlebois, W. H. Smyrl, H. S. White, *J. Electrochem. Soc.* **1994**, *141*, 636–642; c) L. F. Garfias-Mesias, M. Alodan, P. I. James, W. H. Smyrl, *J. Electrochem. Soc.* **1998**, *145*, 2005–2010; d) C. H. Paik, H. S. White, R. C. Alkire, *J. Electrochem. Soc.* **2000**, *147*, 4120–4124; e) I. Serebrennikova, H. S. White, *Electrochem. Solid State Lett.* **2001**, *4*, B4–B6; f) A. Schulte, S. Belger, W. Schuhmann, in *Material Science Forum*, *Vol. 394–395* **"***Shape Memory Materials and its Applications"* (Eds.: Y. Y. Chu, L. C. Zhao), TransTechPublications Ltd., Uetikon-Zürich, **2002**, pp. 145–148.

[6] a) W. B. Nowall, N. Dontha, W. G. Kuhr, *Biosens. Bioelectron.* **1998**, *13*, 1237–1244; b) A. L. Barker, P. R. Unwin, S. Amemiya, J. F. Zhou, A. J. Bard, *J. Phys. Chem. B* **1999**, *103*, 7260–7269; c) J. Zhang, P. R. Unwin, *J. Electroanal. Chem.* **2000**, *494*, 47–52; d) W. J. Miao, Z. F. Ding, A. J. Bard, *J. Phys. Chem. B* **2002**, *106*, 1392–1398.

[7] a) M. Tsionsky, Z. G. Cardon, A. J. Bard, R. B. Jackson, *Plant Physiol.* **1997**, *113*, 895–901; b) T. Yasukawa, Y. Kondo, I. Uchida, T. Matsue, *Chem. Lett.* **1998**, 767–768; c) T. Yasukawa, T. Kaya, T. Matsue, *Anal. Chem.* **1999**, *71*, 4637–4641; d) B. Liu, S. A. Rotenberg, M. V. Mirkin, *Proc. Natl. Acad. Sci. USA* **2000**, *97*, 9855–9860; e) H. Skiku, T. Shiraishi, H. Ohya, T. Matsue, H. Abe, H. Hoshi, M. Kobayashi, *Electrochemistry* **2000**, *68*, 890–892; f) T. Yasukawa, T. Kaya, T. Matsue, *Electroanalysis* **2000**, *12*, 653–659; g) A. Hengstenberg, A. Blöchl, I. D. Dietzel, W. Schuhmann, *Angew. Chem.* **2001**, *113*, 942–946; *Angew. Chem. Int. Ed.* **2001**, *40*, 905—908; h) B. Liu, W. Cheng, S. A. Rotenberg, M. V. Mirkin, *J. Electroanal. Chem.* **2001**, *500*, 590–597; i) H. Shiku, T. Shiraishi, H. Ohya, T. Matsue, H. Abe, H. Hoshi, M. Kobayashi, *Anal. Chem.* **2001**, *73*, 3751–3758; k) C. E. M. Berger, H. Rathod, J. I. Gillespie, B. R. Horrocks, H. K. Datta, *J. Bone Miner. Res.* **2001**, *16*, 2092–2102; l) C. X. Cai, B. Liu, M. V. Mirkin, H. A. Frank, J. F. Rusling, *Anal. Chem.* **2002**, *74*, 114–119.

[8] a) J. Ufheil, F. M. Boldt, M. Borsch, K. Borgwarth, J. Heinze, *Bioelectrochemistry* **2000**, *52*, 103–110; b) I. Turyan, T. Matsue, D. Mandler, *Anal. Chem.* **2000**, *72*, 3431–3435; c) E. M. El-Giar, R. A. Said, G. E. Bridges, D. J. Thomson, *J. Electrochem. Soc.* **2000**, *147*, 586–591; d) S. Gaspar, M. Mosbach, L. Wallman, T. Laurell, E. Csöregi, W. Schuhmann, *Anal. Chem.* **2001**, *73*, 4254–4261.

[9] a) A. L. Barker, M. Gonsalves, J. V. MacPherson, C. J. Slevin, P. R. Unwin, *Anal. Chim. Acta* **1999**, *385*, 223–240; b) M. V. Mirkin, *Mikrochim. Acta* **1999**, *130*, 127–153; c) M. V. Mirkin, B. R. Horrocks, *Anal. Chim. Acta* **2000**, *406*, 119–146; d) G. Nagy, L. Nagy, *Fresenius J. Anal. Chem.* **2000**, *36*, 735–744; e) G. Wittstock, *Fresenius J. Anal. Chem.* **2001**, *370*, 303–315.

[10] a) J. Kwak, A. J. Bard, *Anal. Chem.* **1989**, *61*, 1794–1799; b) R. D. Martin, P. R. Unwin, *Anal. Chem.* **1998**, *70*, 276–284.

[11] D. W. Wipf, A. J. Bard, *Anal. Chem.* **1992**, *64*, 1362–1367.

[12] K. Borgwarth, D. G. Ebling, J. Heinze, *Ber. Bunsenges. Phys. Chem.* **1994**, *98*, 1317–1321.

[13] a) E. Betzig, J. K. Trautmann, T. D. Harris, J. S. Weiner, R. L. Kostelak, *Science* **1991**, *251*, 1468–1470; b) E. Betzig, P. L. Finn, J. S. Weiner, *Appl. Phys. Lett*. **1992**, *60*, 2484–2486.

[14] a) M. Ludwig, C. Kranz, W. Schuhmann, H. E. Gaub, *Rev. Sci. Instr.* **1995**, *66*, 2857–2860; b) C. Kranz, H. E. Gaub, W. Schuhmann, *Adv. Mater.* **1996**, *8*, 634–637; c) A. Hengstenberg, C. Kranz, W. Schuhmann, *Chem. Eur. J.* **2000**, *6*, 1547–1554.

[15] a) P. I. James, L. F. Garfias-Mesias, P. J. Moyer, W. H. Smyrl, *J. Electrochem. Soc*. **1998**, *145*, L64–L66; b) M. Büchler, S. C. Kelly, W. H. Smyrl, *Electrochem. Solid-State Lett.* **2000**, *3*, 35–38.

[16] a) M. A. Alpuche-Alviles, D. O. Wipf, *Anal. Chem*. **2001**, *73*, 4873–4881; b) B. Ballesteros Katemann, A. Schulte, E. J. Calvo, M. Koudelka-Hep, W. Schuhmann. *Electrochem. Commun.* **2002**, *4*, 134–138.

[17] a) J. V. MacPherson, P. R. Unwin, *Anal. Chem.* **2000**, *72*, 276–285; b) C. Kranz, G. Friedbacher, B. Mizaikoff, *Anal. Chem.* **2001**, *73*, 2491–2500; c) J. V. MacPherson, P. R. Unwin, *Anal. Chem.* **2001**, *73*, 550–557; d) A. Lugstein, E. Bertagnolli, C. Kranz, B. Mizaikoff, *Surf. Interface Anal.* **2002**, *33*, 146–150; e) J. V. MacPherson, J. P. G. de Mussy, J. L. Delplancke, *J. Electrochem. Soc.* **2002**, *149*, B306–B313; f) J. V. MacPherson, C. E. Jones, A. L. Barker, P. R. Unwin, *Anal. Chem.* **2002**, *74*, 1841–1848.

[18] a) R. Brunner, A. Bietsch, O. Hollricher, O. Marti, *Rev. Sci. Instrum.* **1997**, *68*, 1769–1772; b) O. Hollricher, R. Brunner, O. Marti, *Ultramicroscopy* **1998**, *71*, 143–147.

[19] a) Y. H. Shao, M. V. Mirkin, G. Fish, S. Kokotov, D. Palanker, A. Lewis, *Anal. Chem.* **1997**, *69*, 1627–1634; b) P. Sun, Z. Q. Zhang, J. D. Guo, Y. H. Shao, *Anal. Chem.* **2001**, *73*, 5346–5351; c) B. Ballesteros Katemann, W. Schuhmann, *Electroanalysis* **2002**, *14*, 22–28.

Received: July 22, 2002

Revised: December 20, 2002 [F4267]

  